

A Single-Mode, Self-Adapting, and Self-Powered Mechanoreceptor Based on a Potentiometric–Triboelectric Hybridized Sensing Mechanism for Resolving Complex Stimuli

Xiaodong Wu, Juan Zhu, James W. Evans, and Ana C. Arias*

Human skin is equipped with slow adapting (SA) and fast adapting (FA) capabilities simultaneously. To mimic such functionalities, elaborately designed devices have been explored by integrating multiple sensing elements or adopting multimode sensing principles. However, the complicated fabrication, signal mismatch of different modules, complex operation, and high power-consumption hinder their widespread applications. Here, a new type of single-mode and self-powered mechanoreceptor that can mimic both SA and FA via seamless fusion of complementary while compatible potentiometric and triboelectric sensing principles is reported. The resultant potentiometric–triboelectric hybridized mechanoreceptor exhibits distinctive features that are hard to achieve via currently existing methods, including single-mode output (only voltage signal), greatly simplified operation (single-measurement setup), ultralow power-consumption (<1 nW), self-adaptive response behavior, and good capability for resolving complex stimuli. Diverse mechanical characteristics, including magnitude, duration, frequency, applying and releasing speed, can be well interpreted with this single-mode and self-powered mechanoreceptor. Its promising application for monitoring object manipulations with a soft robotic gripper is explored. Furthermore, the versatility of the mechanoreceptor for resolving complex stimuli in diverse daily scenarios is demonstrated. This work presents a new design that will significantly simplify the fabrication/operation and meanwhile boost the functionality/energy-efficiency of future electronic devices and smart systems.


SA mechanoreceptors (e.g., Merkel disk and Ruffini cylinder) are distributed near the skin surface and can produce sustained signals in response to static touch or pressure (Figure 1a). FA mechanoreceptors (e.g., Meissner corpuscle and Pacinian corpuscle) respond only at the beginning and/or ending moments of stimulation and can detect dynamic vibration or sliding (Figure 1a). To mimic these functions of human skin, artificial sensors have been developed utilizing different sensing mechanisms. Particularly, resistive, capacitive, and transistor-based sensors are suitable to mimic SA mechanoreceptors as they can maintain the signal produced by a static stimulus,^[4–6] whereas triboelectric and piezoelectric sensors can generate instantaneous signal output and are capable of mimicking FA mechanoreceptors.^[1,7] Nevertheless, sensors based on a single sensing mechanism have only one type of signal output with limited information interpreted, restricting the scenarios of their practical applications.

To meet the requirement for resolving complex stimuli in the emerging fields of artificial prosthetics, humanoid robotics, and wearable healthcare devices, sensing

Natural skin sensory systems can perceive complex mechanical stimuli and enable us to interact with the surrounding environment effectively and efficiently. Typically, there are two categories of mechanoreceptors in human skin: slow adapting (SA) mechanoreceptors and fast adapting (FA) mechanoreceptors.^[1–3]

Dr. X. Wu, Dr. J. Zhu, Prof. A. C. Arias
Department of Electrical Engineering and Computer Sciences
University of California
Berkeley, CA 94720, USA
E-mail: acarias@eecs.berkeley.edu

Prof. J. W. Evans
Department of Materials Science and Engineering
University of California
Berkeley, CA 94720, USA

 The ORCID identification number(s) for the author(s) of this article can be found under <https://doi.org/10.1002/adma.202005970>.

DOI: 10.1002/adma.202005970

devices that can imitate both SA and FA functions are in high demand. Numerous efforts have been made to approach this goal in recent years and two major strategies have been developed. One strategy is spatial integration of different sensing elements into one platform.^[8–12] For example, a fingertip-like sensor that can discriminate lateral sliding and vertical pressure is developed by spatially combining triboelectric and piezoresistive sensing elements.^[8] Besides, a self-powered sensor for mimicking SA and FA has been developed based on spatial integration of an ion-channel system and a piezoelectric film.^[10] This spatial integration strategy is straightforward and the individual sensing elements can work independently. Nevertheless, the fabrication processes are complicated and the devices are bulky. Another strategy is the merging of different sensing principles to fabricate multimode sensing devices.^[13–18] For instance, flexible sensors that can detect different mechanical stimuli (e.g., pressure, strain, flexion, etc.) have been developed.^[13,14] In

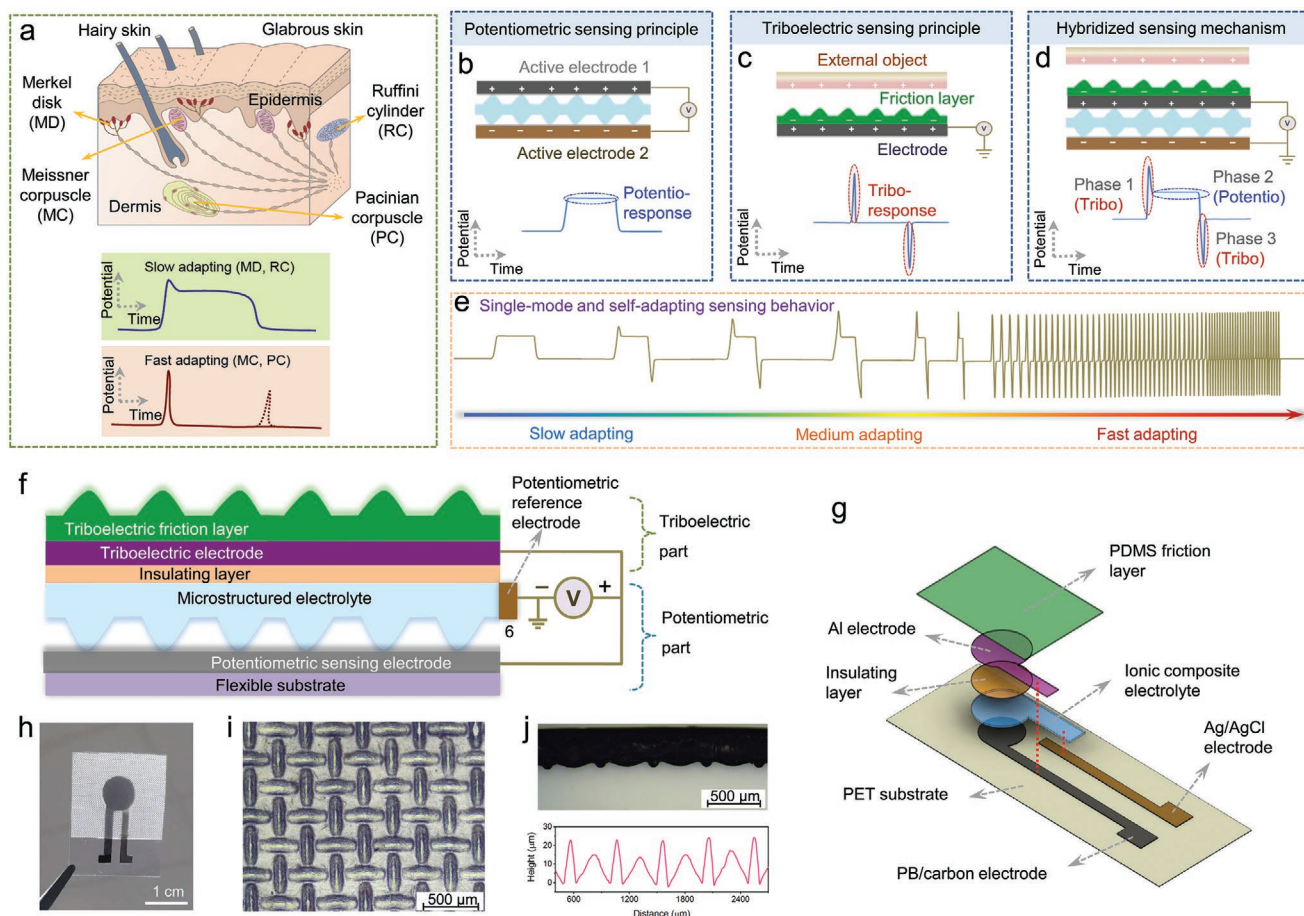


Figure 1. Design and configuration of the potentiometric–triboelectric hybridized mechanoreceptor. a) Illustrations showing the distribution and response behaviors of SA and FA mechanoreceptors in natural skin. b–d) Schematic diagrams depicting the configurations and typical signal outputs of a potentiometric sensing device, triboelectric sensing device, and potentiometric–triboelectric hybridized sensing device. e) Illustration showing the self-adapting response behavior of the mechanoreceptor to different types of mechanical stimuli. f) Schematic depicting the configuration design of the mechanoreceptor. g) Illustration showing the structure layout of the mechanoreceptor. h) Photograph of the fabricated mechanoreceptor. i, j) Optical microscopy image, cross-sectional morphology, and surface profile of the microstructured ionic composite used in the mechanoreceptor.

addition, a sensor that can detect static and dynamic pressure based on piezoresistive and piezoelectric sensing mechanisms is reported.^[15,18] These multimode sensors are easier to fabricate and are more compact compared with the spatially integrated sensing platforms. However, the main drawback of these devices is that their multiple sensing modes cannot be operated concurrently due to the mutual interference/crosstalk between them, making them incapable of simultaneously detecting and thus discriminating different types of stimuli.

Additionally, for the aforementioned complex sensing devices, the signal outputs from different sensing modules are normally not compatible with each other, which necessitates different measurement setups or signal converters to record and process all of the data. As a result, the data acquisition speed is compromised because of the repeated switching between different sensing modules. Also, the power-consumption is increased due to the necessity of multiple measurement setups or signal conversion equipment. Therefore, how to simplify the operation of sensing devices while boost their functionality and energy-efficiency remains a great challenge yet an exciting goal in the burgeoning field of human–machine interaction.

Here, for the first time, we present a new mechanotransduction mechanism through seamlessly hybridizing complementary while compatible potentiometric and triboelectric sensing principles, resulting in a single-mode, self-adapting, and self-powered mechanoreceptor with good capability of resolving complex mechanical stimuli. Compared to the currently existing sensing devices (Table S1, Supporting Information), the mechanoreceptor presented in this work features five distinctive characteristics: 1) greatly simplified operation and measurement benefiting from the single-mode signal output (i.e., only voltage output); 2) self-generated voltage output and ultralow power-consumption (<1 nW); 3) a novel self-adaptive response behavior (i.e., self-regulated operating principle according to the characters of external stimuli); 4) good capability for not only detection but also discrimination of both static and dynamic stimuli; and 5) solution-processing-based fabrication and large-scale manufacturing feasibility. The promising application of the mechanoreceptor for monitoring object manipulations with a soft robotic gripper is explored. Additionally, we demonstrate several special scenarios of this mechanoreceptor in resolving diverse mechanical stimuli in our daily life. With the

distinctive merits of simplified fabrication/operation, enhanced sensing capability, and boosted energy-efficiency, this new type of single-mode and self-adapting mechanoreceptor is very intriguing for practical applications in biomimetic robots, artificial prosthetics, healthcare devices, and other smart systems.

We first clarify the design philosophy of the potentiometric-triboelectric hybridized mechanotransduction mechanism. The potentiometric sensing principle enables encoding a mechanical stimulus into continuous voltage output (Figure 1b, see Figures S1 and S2 in the Supporting Information for detailed discussion).^[19] Briefly, a microstructured electrolyte is placed between two active electrodes. Applying a force on the device increases the contact area between the electrolyte and electrodes, leading to a variation in the potential difference output measured between the two electrodes. Devices based on this potentiometric sensing mechanism can only be used to detect static or slowly varying stimuli. In contrast, devices based on triboelectric sensing mechanism only give instantaneous voltage output at the beginning and ending moments of stimulation (Figure 1c, see Figure S3 in the Supporting Information for detailed discussion), making them selectively sensitive to dynamic stimuli.^[1,7] Notably, these two sensing mechanisms are complementary in the targeted stimulus type (one for static and the other for dynamic) while they are compatible in signal output (both with voltage output). This makes it feasible to hybridize their signal outputs and create a single-mode yet multifunctional mechanoreceptor. With this concept in mind, we report a device structure with a hybridized sensing mechanism as illustrated in Figure 1d. The single-mode signal output of the hybridized mechanoreceptor exhibits both potentiometric and triboelectric characteristics. Typically, a hybridized signal pattern can be described into three phases: 1) an instantaneous voltage upswing when applying a stimulus, 2) a sustained voltage plateau while holding the stimulus, and 3) an instantaneous voltage decline when the stimulus is released. Phase 1 and phase 3 come from the triboelectric sensing principle and reflect the dynamic features such as frequency, applying speed, and threshold of the stimulus. Phase 2 arises from the potentiometric sensing principle and reveals the static characteristics such as magnitude and duration of the stimulus. The hybridization of these two signals provides rich information and more completed interpretation of the applied stimulus.

Interestingly, the operating principle of the mechanoreceptor can be switched autonomously according to the characters of the external stimuli, featuring a novel self-adapting sensing behavior. As depicted in Figure 1e and shown in Movie S1 (Supporting Information), when applying a static stimulus on the device slowly, the potentiometric sensing principle mainly contributes to the signal output while the triboelectric sensing principle has little impact. Thus, only a sustained signal output can be detected. When applying a medium-speed stimulus on the device, the potentiometric and triboelectric sensing principles respond simultaneously and generate a hybridized signal output. Both static and dynamic characteristics of the stimulus can be reflected from the hybridized signal as mentioned above. When applying a rapidly varying stimulus on the device, only the triboelectric sensing principle can respond with a major contribution to the signal output. Such single-mode output and self-adapting

behavior allow us to greatly simplify the operation and enhance the functionality of mechanical sensing devices.

The configuration design of the mechanoreceptor is illustrated in Figure 1f. The mechanoreceptor can be regarded as two parts: a triboelectric and a potentiometric part. The triboelectric part employs a single-electrode sensing configuration with a microstructured friction layer placed on the top of an electrode layer.^[20–23] The potentiometric part is formed by a microstructured electrolyte, a reference electrode, and a sensing electrode. One end of the electrolyte is fully connected to the reference electrode and the microstructured side is set against the sensing electrode. Changing the contact area between the microstructured electrolyte and the sensing electrode will regulate the voltage output measured between the two electrodes.

The structure layout of the mechanoreceptor is illustrated in Figure 1g and the fabrication process is shown in Figure S4 (Supporting Information). Poly(dimethylsiloxane) (PDMS), one of the most triboelectric negative materials,^[24,25] is used to prepare the friction layer for the triboelectric part and a microstructure is created on the surface to enhance the triboelectric effect (Figure S5, Supporting Information). Thin aluminum (Al) foil ($\approx 20 \mu\text{m}$) is used to prepare the triboelectric electrode layer. Prussian blue modified graphite carbon (PB/carbon) and silver/silver chloride (Ag/AgCl) are employed as the sensing electrode and the reference electrode respectively for the potentiometric part. These electrodes are stencil-printed on a flexible poly(ethylene terephthalate) (PET) substrate. A microstructured poly(vinyl alcohol)/sodium chloride/glycerol (PVA/NaCl/Gly) ionic composite prepared via a mesh-molding strategy (Figure S6, Supporting Information) is used as the electrolyte. The microstructured ionic composite is placed on the PB/carbon electrode, with one end of the ionic composite fully connected to the Ag/AgCl electrode (as the red dashed line shows in Figure 1g). The Al electrode is connected with the PB/carbon electrode via conductive paste (as the red dashed line shows in Figure 1g). An insulating layer is set between the ionic composite and the Al electrode. The top PDMS friction layer also serves as an encapsulating layer for the whole device. The final device is shown in Figure 1h. The morphology and surface profile of the microstructured ionic composite is shown in Figure 1i,j. For the operation of this mechanoreceptor (Figure S7, Supporting Information), the triboelectric electrode and the potentiometric sensing electrode are connected to the positive terminal of the measurement setup, and the potentiometric reference electrode is connected to the negative measurement terminal.

Figure 2a,b shows the measured signal output of the mechanoreceptor when it is operated in potentiometric mode only. The output of the triboelectric mode is shown in Figure 2c,d, and the combined signal from hybridized mode is shown in Figure 2e,f. The potentiometric sensing mode gives a sustained response to the stimulation while the triboelectric sensing mode generates instantaneous signal outputs at the beginning and ending moments of the stimulation (Figure 2b,d, and Figure S8a,b, Supporting Information). The signal output of the hybridized mode (with two triboelectric spikes and a potentiometric plateau) inherits the characteristics of both potentiometric and triboelectric signals (Figure 2f and Figure S8c, Supporting Information), which illustrates the compatibility

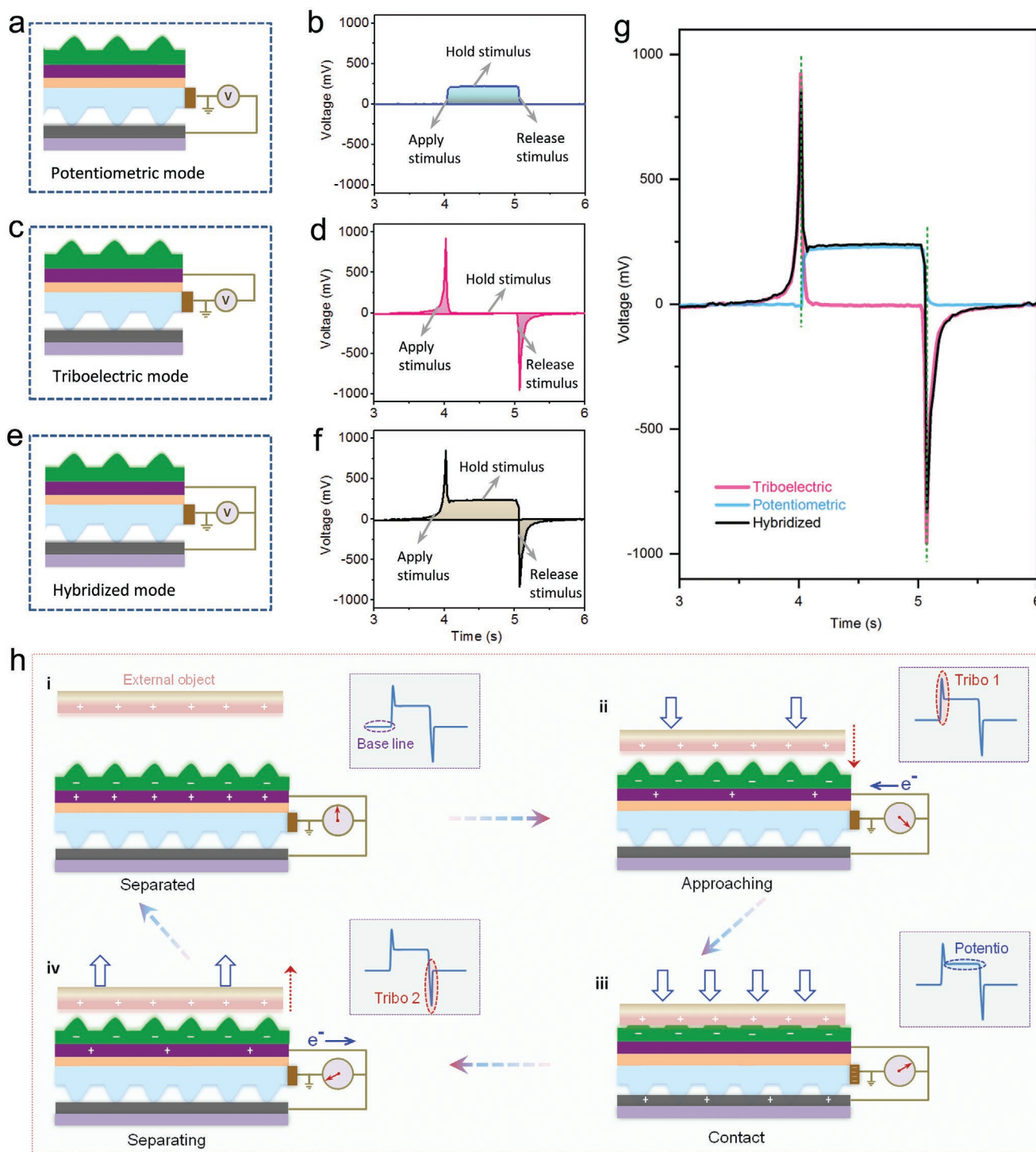


Figure 2. Working mechanism of the hybridized mechanoreceptor. a–f) Illustrations showing configurations and signal outputs of the mechanoreceptor operated in potentiometric mode (a,b), triboelectric mode (c,d), and hybridized mode (e,f), respectively. g) Temporal relations between potentiometric mode, triboelectric mode, and hybridized mode in response to an identical stimulus, revealing the hybridization principle. h) Schematics show the working principle of the hybridized sensing mechanism, which involves the beginning separated state (i), approaching process (ii), pressed status (iii), and separating process (iv).

and autonomy of the potentiometric and triboelectric sensing processes (see Figures S9 and S10 in the Supporting Information for detailed discussion).

The temporal relationship between the potentiometric, triboelectric, and hybridized signal outputs is shown in Figure 2g. The applied stimulus on the hybridized mechanoreceptor first

generates a triboelectric spike, followed by the generation of a potentiometric plateau. This is due to the sensor design, where the triboelectric part of the mechanoreceptor is on the top of the potentiometric part as shown in Figure 1f. The external stimulus is first received by the upper triboelectric layer and then transferred to the potentiometric layer placed on the bottom of the device. In addition, the triboelectric sensing mode responds to the approaching of and touching with the external object as illustrated in Figure 2h, while the potentiometric sensing mode is more related to the compressive strain induced by the external force. Thus, the potentiometric signal will always be observed after the triboelectric spike output. Conversely, when releasing the applied stimulus from the mechanoreceptor, a reversed process is observed. The potentiometric plateau vanishes firstly, followed by the generation of an opposite triboelectric spike signal. The hybridization of these two autonomous and complementary sensing modes results in a single-mode and versatile mechanotransduction mechanism.

The working mechanism of the hybridized mechanoreceptor is illustrated in Figure 2h. During the contact and friction process, electrons transfer from the external object to the PDMS friction layer due to triboelectrification effect, generating opposite electrostatic charges on the two surfaces. With the object separated from the friction layer, the negative charges on the friction layer induce positive charges on the triboelectric electrode layer due to electrostatic induction effect, resulting in a steady-state without signal output (Figure 2h–i). When the object is approaching the PDMS friction layer again, the induced positive charges on the electrode layer decrease and electrons flow back to the triboelectric electrode, leading to a prompt voltage upswing (Figure 2h–ii).^[20,22,26] As the object comes into full contact with the PDMS friction layer, the charges on the object and friction layer are fully balanced/screened (Figure 2h–iii), reaching another steady-state without triboelectric signal output. However, the potentiometric mode is activated at this moment by the applied force from the object, generating a sustained potentiometric output (Figure 2h–iii). When the object is separating from the device, the potentiometric output is cut off gradually. However, positive charges generate on the triboelectric electrode layer due to electrostatic induction effect, resulting in a reversed triboelectric spike (Figure 2h–iv). With the object totally separated from the mechanoreceptor, the device goes back to the initial steady-state (Figure 2h–i). When repeatedly applying a stimulus to the mechanoreceptor, the processes in Figure 2h are repeatable, generating periodic signal outputs (Figure S8c, Supporting Information).

The response behavior of the mechanoreceptor to mechanical stimuli of different frequencies is shown in Figure 3a and Movie S1 (Supporting Information). When slowly applying a stimulus (≈ 5 N) on the mechanoreceptor, potentiometric signal output is generated gradually and is maintained when holding the stimulus, exhibiting a slow adapting behavior. Upon increasing the stimulus frequency, two triboelectric sharp spikes appear when applying and releasing the stimulus, with the magnitude of the spike increasing with the stimulus frequency. When further elevating the stimulus frequency, the potentiometric output is gradually suppressed by the triboelectric spike signals, showing a fast adapting sensing behavior.

This novel self-adapting sensing principle endows the mechanoreceptor with the capability for detecting as well as discriminating both static and dynamic stimuli.

The influence of stimulus magnitude and stimulus applying speed on the response behavior of the mechanoreceptor is shown in Figure 3b. By increasing the magnitude of the mechanical stimulus, both potentiometric and triboelectric outputs are higher as depicted in Figure 3c. For the potentiometric sensing principle, larger stimulus gives rise to a larger contact area between the electrolyte and the sensing electrode, resulting in higher measured voltage output. For the triboelectric sensing principle, larger stimulus augments the triboelectrification process, which can generate more triboelectric charges and give higher triboelectric output.^[27,28] By increasing the stimulus applying speed, as shown in Figure 3d, the triboelectric output is enhanced significantly while the potentiometric output exhibits an inconspicuous variation. This is because higher stimulus applying speed can accelerate the electrostatic induction processes (i.e., approaching and separating processes in Figure 2h), resulting in stronger signal outputs.^[29–31] The potentiometric output mainly depends on the electrolyte deformation induced by the stimulus. The aforementioned phenomena observed on the hybridized mechanoreceptor are also observed on the potentiometric and triboelectric sensing parts (Figure S11, Supporting Information). The sensitivity of the potentiometric mode and triboelectric mode to mechanical stimulations is calculated to be ≈ 17 and ≈ 20 mV N⁻¹ respectively (Figure 3c). The detection range of the mechanoreceptor is measured to be 0.01–10 N, as revealed from Figure 3f and Figure S1c (Supporting Information).

The single-mode signal output of the mechanoreceptor provides important information about the mechanical stimulus. As depicted in Figure 3e, the magnitude (F) of the stimulus can be obtained from the height of the potentiometric output plateau. The duration (t) of the stimulus can be measured from the width of the potentiometric plateau. The stimulus frequency (f) can be calculated from the time difference between two typical signal patterns. Additionally, the stimulus applying (v_1) and releasing (v_2) speeds can be reflected from the two triboelectric peaks (p_1 and p_2). More importantly, the potentiometric sensing principle and the triboelectric sensing principle can compensate for the deficiencies of each other. Specifically, when the mechanoreceptor is under a critical point of contact (0.01 N)/noncontact (0 N) with an external object, the potentiometric sensing principle is not activated yet while the triboelectric sensing principle enables to detect this subtle variation and generates weak triboelectric spikes (Figure 3f). On the other hand, when the mechanoreceptor is pretouched by an external object and then the stimulus magnitude changes, the triboelectric sensing principle is restrained by the pre-touching since charge transfer/separation will not occur. However, the potentiometric sensing principle is activated and can monitor the magnitude variation of the stimulus (Figure 3g). Such complementation of these two sensing principles can greatly extend the application range of the hybridized mechanoreceptor.

Compared with the currently existing complex sensing devices (Table S1, Supporting Information), this single-mode and self-adapting mechanoreceptor exhibits significant

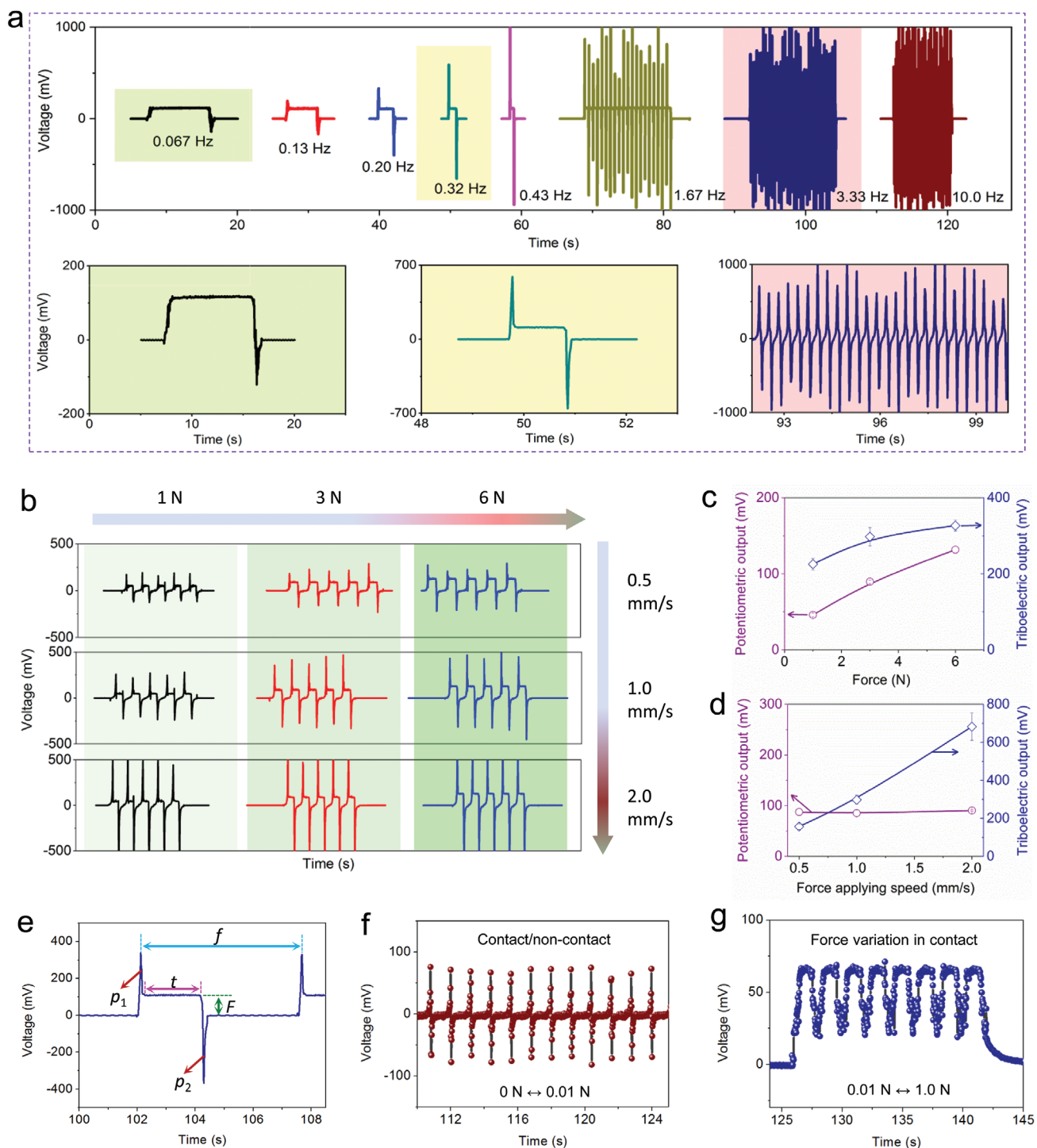


Figure 3. Sensing performance of the mechanoreceptor. a) Signal outputs of the mechanoreceptor when subjected to mechanical stimuli (≈ 5 N) of varying frequency. b) Response behaviors of the mechanoreceptor when subjected to different stimulus magnitudes and stimulus applying speeds. c,d) Extracted triboelectric output and potentiometric output under different stimulus magnitudes and stimulus applying speeds. e) Typical signal pattern of the mechanoreceptor, from which rich information (e.g., F , t , f , ν_1 and ν_2) can be reflected/extracted. f) Signal output of the mechanoreceptor under a critical point of contact (0.01 N)/noncontact (0 N) with an external object. g) Signal output of the mechanoreceptor when it is pre-touched first, followed by changing the stimulus magnitude from 0.01 to 1.0 N repeatedly.

advantages in terms of device fabrication (solution processing-based), simplified operation/measurement (single-mode signal output and single measurement equipment), self-generated

voltage output, and resolution of complex stimuli (both SA and FA), which are challenging to achieve but are highly desirable for constructing a wide range of sensing devices and systems.

Compared with conventional rigid robotic hands, soft robotic hands feature high mechanical compliance and enable safer and more efficient manipulation of objects. Proprioceptive sensory capability is a prerequisite for agile grasping and dexterous object manipulation.^[32,33] Integration of easily operated, multifunctional, and energy-saving mechanical sensors with soft robotic hands can remarkably enhance their accuracy, efficiency, and versatility. The presented mechanoreceptor in

this work enables resolving complex mechanical stimuli via a self-powered manner and simplified operation, exhibiting good promise for the construction of agile robotic hands with sensory functions. As a proof of concept, we designed and fabricated a soft robotic gripper with three fingers, as shown in **Figure 4a** (see Figure S12 in the Supporting Information for the fabrication process). The robotic gripper, which mainly consists of soft-bodied fluid channels and a strain-limiting layer, can

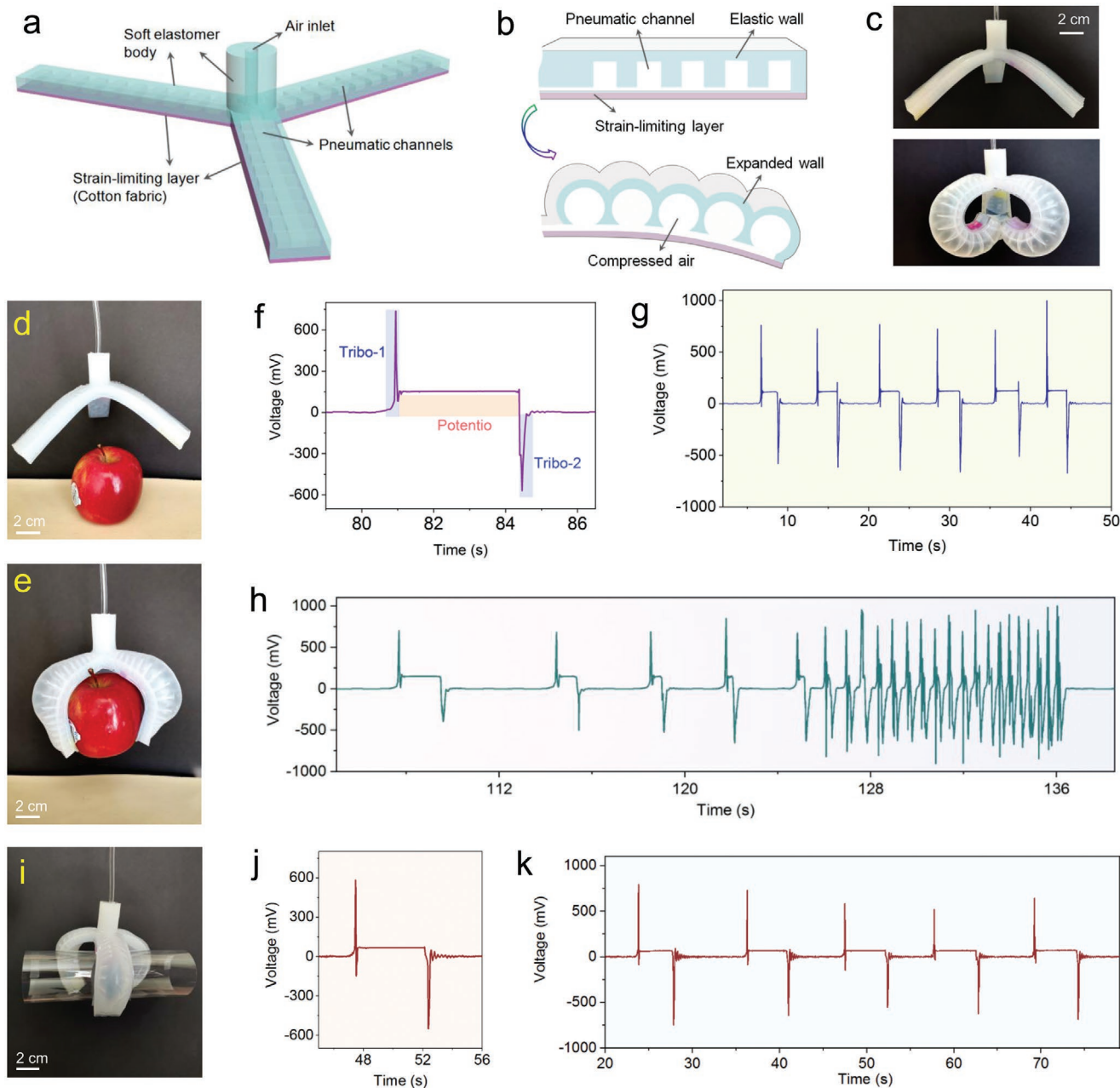


Figure 4. Soft robotic gripper with mechanoreceptor for resolving complex stimuli. a,b) Schematic diagrams illustrating the structural layout of the soft robotic gripper and its operating principle based on pneumatic actuation. c) Photographs of the soft robotic gripper at the unpressurized state and pressurized state. d,e) Photographs showing the manipulation of an apple using the soft robotic gripper. f,g) Recorded signal outputs of the mechanoreceptor installed on the soft gripper finger during repeated manipulation of the apple. h) Signal output of the mechanoreceptor when performing “pick-and-place” operations of the apple with varying frequency. i–k) Photograph and recorded signal outputs of the soft robotic gripper when grasping–releasing a plastic film roll (PET film, 125 μm thick).

be pneumatically actuated, as illustrated in Figure 4b. When pressurized, the pneumatic channels expand and the gripper fingers bend towards the strain-limiting layer. So, the entire robotic gripper can be actuated and controlled with compressed air (Figure 4c). We attached our mechanoreceptor to the fingers of the robotic gripper to monitor the mechanical stimuli in real time when performing “pick–hold–place” operations of different objects. As shown in Figure 4d,e, an apple can be easily manipulated with this soft robotic gripper. From the recorded signal outputs of the integrated mechanoreceptor (Figure 4f,g), the “pick” operation generated a positive triboelectric peak, while the “place” operation gave rise to a reversed negative triboelectric peak. When holding the apple steadily, the signal output of the mechanoreceptor kept stable, which comes from the potentiometric mode of the mechanoreceptor. As the frequency of these operations increases continuously, the picking, holding, and placing processes can be clearly recognized from the recorded signal outputs of the mechanoreceptor (Figure 4h).

In addition, we investigated the response signals of the mechanoreceptor when grasping a deformable object. As an example, a roll of thin plastic film was used, which can be deformed by the applied force (Figure 4i). Notably, the potentiometric plateau generated when holding the thin plastic film roll is relatively lower than that of the apple holding operation (Figure 4j,k). This is because the plastic film roll is lighter than the apple. The applied force on the plastic film roll is smaller than that applied on the apple. Also, when the plastic film roll was released, a signal damping process was observed, which can be attributed to the enhanced vibration of the gripper fingers by the shape recovery process of the plastic film roll. The rich information extracted with this mechanoreceptor provides new opportunities for the realization of agile and dexterous object manipulations using soft robotic hands.

With good capability to mimic both SA and FA, this presented mechanoreceptor can be used to resolve complex stimulations in our daily life. For example, the keys on the keyboard are designed to have different functions and the way we press them is also different. Here, we demonstrate the keystroke habit with this mechanoreceptor. We find that a noticeable difference between keystrokes is the “Ctrl” key and the “Enter” key (Figure 5a). For the “Ctrl” key, the keystroke duration is relatively long (≈ 0.7 s, Figure 5b). In contrast, for the “Enter” key, the keystroke is very fast (only ≈ 0.1 s) and almost instantaneous (Figure 5c). The keystroke behavior presented by different people is also different and this mechanoreceptor would be a useful tool to analyze such human user behavior.

Another distinctive characteristic of this mechanoreceptor is its capability to simultaneously detect both static and dynamic stimuli. As a demonstration, a mechanoreceptor is fixed to the wrist with tape (Figure 5d). When bending the wrist, a continuous potentiometric signal output is recorded (Figure 5e) due to the vertical pressure induced by the wrist bending. Interestingly, during repeatedly pressing the mechanoreceptor after the wrist bending, additional triboelectric spikes are detected on the basis of the pristine potentiometric signal, benefiting from the good compatibility and autonomy of these two sensing principles. These results verify that this single-mode mechanoreceptor can be used to detect both static and dynamic stimuli and can also discriminate them.

Finally, we demonstrate that the mechanoreceptor is qualified to monitor dynamic mechanical vibrations. The mechanoreceptor is fixed onto one end of a plastic board (≈ 2 mm thick) and then we apply a gentle knock to the other end of the plastic board (≈ 40 cm away from the mechanoreceptor) to generate a mechanical vibration (Figure 5f). The mechanical vibration can be monitored in real time by the mechanoreceptor (Figure 5g). Remarkably, the damping process of the vibration can be clearly recognized in Figure 5h. Additionally, we attach a mechanoreceptor to a speaker to detect the vibration when playing music (Figure 5i). As shown in Figure 5j, the diaphragm vibration of the speaker can be recorded continuously with this mechanoreceptor. These results demonstrate the good capability of this mechanoreceptor for detecting dynamic mechanical vibrations.

In summary, we have demonstrated a new type of mechanoreceptor based on a potentiometric–triboelectric hybridized sensing mechanism. This mechanoreceptor features a single-mode signal output and a self-adapting sensing behavior, which can greatly simplify the device operation and the measurement circuitry. More importantly, this self-adapting sensing mechanism enables us to detect both static and dynamic mechanical stimuli and also allows us to discriminate them. Furthermore, the voltage output of the mechanoreceptor is totally self-generated without external power supply. Several special application scenarios of the mechanoreceptor in detecting diverse mechanical stimuli are also demonstrated. Such single-mode and self-adapting sensing style presented in this work achieves an unprecedented economical efficiency given the simplified fabrication/operation, boosted functionality, and enhanced energy-efficiency, opening up great opportunities for creating a new range of smart electronic devices and systems.

Experimental Section

Printing of PB/Carbon and Ag/AgCl Electrodes: Kapton tape films (60 μm thick) were cut into defined patterns via laser-cutting and attached to 125 μm thick and flexible PET substrate as stencils for stencil printing of the electrodes. PB/carbon ink (C2070424P2, Gwent Electronic Materials Ltd.) was first stencil printed on the PET substrate using a glass slide, followed by drying the ink at 100 $^{\circ}\text{C}$ for 10 min. Then, Ag/AgCl ink (CI-4001, Engineered Materials Systems, Inc.) was stencil printed on the substrate as another electrode. Both electrodes were then cured at 130 $^{\circ}\text{C}$ for 1 h. After removing the Kapton film stencil, PB/carbon sensing electrode and Ag/AgCl reference electrode with defined patterns were prepared. Finally, the surfaces of the PB/carbon electrode and Ag/AgCl electrode were polished and cleaned with wiping paper (TechniCloth, Texwipe Company) dipped with ethanol to remove the additives of the inks left on the surface, thus to obtain a clear and stable electrode surface.

Preparation of Microstructured PVA/NaCl/Gly Ionic Composite and PDMS Friction Layer: The microstructured PVA/NaCl/Gly ionic composite was prepared using a solution casting method (Figure S6, Supporting Information). Specifically, PVA/NaCl/Gly aqueous solution composing of 25 wt% PVA, 100×10^{-3} M NaCl, and Gly (the weight ratio of Gly to PVA is 0.24) was prepared and degassed by standing for 24 h. Then, this aqueous solution was cast onto a micropatterned template that was fabricated via a mesh-molding strategy. The cast PVA/NaCl/Gly solution was dried in a fume hood at ambient temperature for 48 h. After drying, the PVA/NaCl/Gly ionic composite film (≈ 600 μm in thickness) was peeled off from the template, with uniform and periodic microstructure created on the surface. The PDMS friction layer (≈ 350 μm in thickness) with a similar microstructure was also prepared based on a mesh-molding strategy (Figure S5, Supporting Information).^[34]

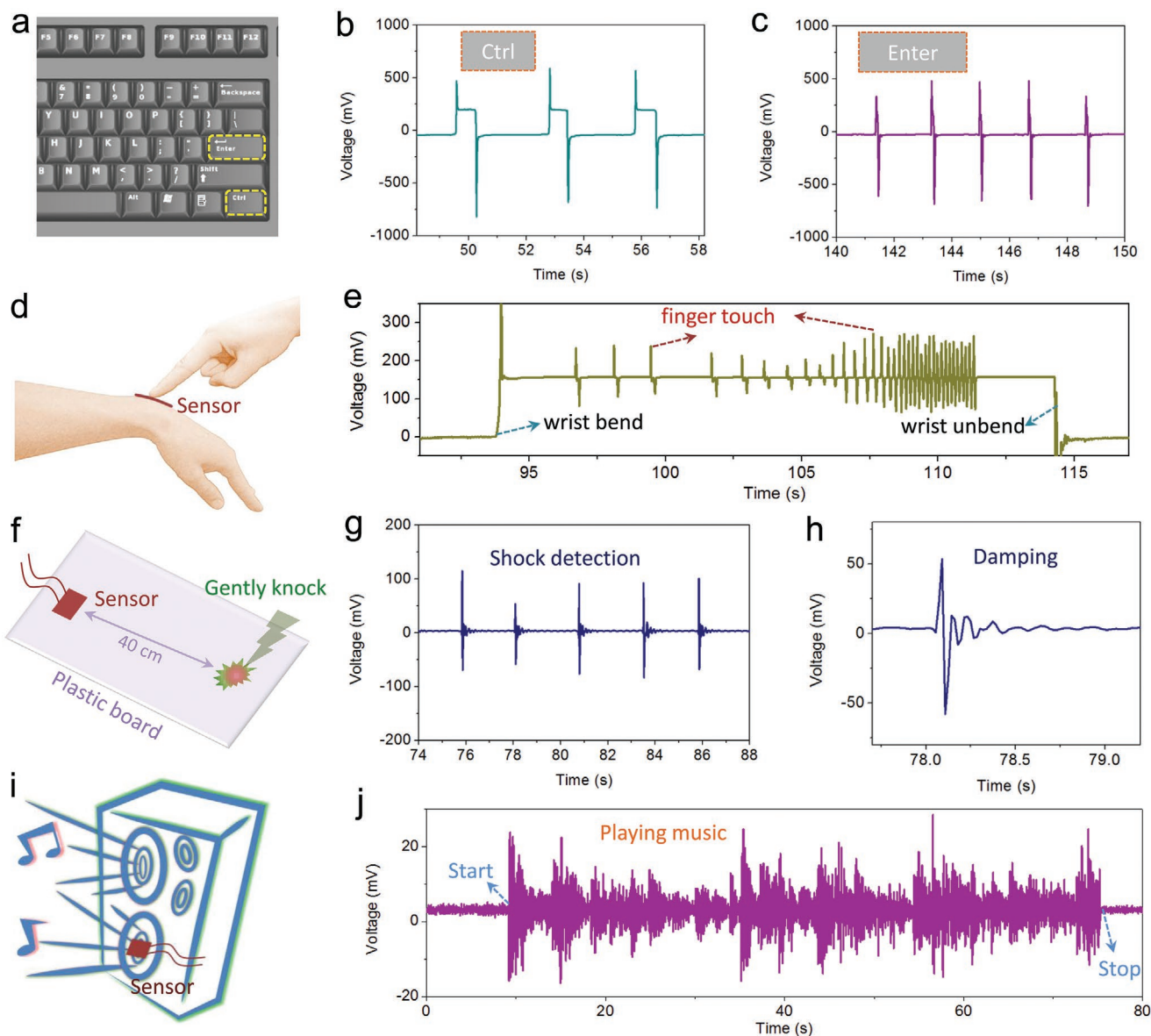


Figure 5. Applications of the mechanoreceptor for resolving complex stimuli in our daily life. a–c) Response behaviors of the mechanoreceptor when pressing the “Ctrl” and “Enter” keys to investigate the keystroke habit. d,e) Illustration and response signal of a mechanoreceptor attached to the wrist. The wrist is first bent to apply a static stimulus, followed by pressing the mechanoreceptor rapidly to apply an additional dynamic stimulus. f–h) Application of the mechanoreceptor for detecting the mechanical vibration of a plastic board. i,j) Recorded signal of a mechanoreceptor fixed on a speaker during playing music.

Fabrication of the Hybridized Mechanoreceptor: The whole fabrication process of the mechanoreceptor is shown in Figure S4 (Supporting Information). The PB/carbon sensing electrode and Ag/AgCl reference electrode were printed on a flexible PET substrate as mentioned above. Laser cutting was used to define the pattern of the PVA/NaCl/Gly ionic composite. A small patch of paper tape (2 mm × 3 mm × 0.14 mm), which acts as a spacer for the ionic composite and the PB/carbon electrode, was placed between the Ag/AgCl electrode and the sensing region of the PB/carbon electrode. Then, PVA/NaCl/Gly aqueous solution (the weight ratio of Gly to PVA is 0.24) was pasted to the Ag/AgCl electrode as a glue near the sensing region, followed by fixing one end of the PVA/NaCl/Gly ionic composite (in the shape of “q”) to the Ag/AgCl electrode (as the dashed red line shows in Figure S4, Supporting Information). The whole device was placed into an environmental chamber and dried for 12 h at 25 °C and 35% RH. Afterward, a double-sided adhesive tape

(≈100 μm thick) was cut into a defined shape and placed on the top of the PVA/NaCl/Gly ionic composite as an insulating layer. Then, a 20 μm thick aluminum foil (in the shape of the letter “p”), which acts as the triboelectric electrode layer, was placed onto the adhesive insulating layer. The triboelectric electrode was then connected to the potentiometric sensing electrode (as the dashed red line shows in Figure S4 in the Supporting Information). Finally, the whole device was encapsulated with a microstructured PDMS layer. The microstructured PDMS layer also serves as the triboelectric friction layer, since PDMS is one of the most negative materials (i.e., easy to gain electrons during friction) in the triboelectric series. The microstructure was created on the PDMS layer to avoid the adhesion with external objects and also to enhance the triboelectric effect.^[22,35,36]

Characterization and Measurement: Optical microscopy observation was conducted on a microscope (Eclipse 50i, Nikon). A Dektak profiler

(Veeco 6M) was used for the profile measurement. SEM observation was carried out on a Zeiss microscope with EHT value of 5 kV. The voltage signal output of the mechanoreceptor was collected with a digital source meter (Keithley 2601A) using a voltage measure-only mode (sourcing nearly zero current and measuring the voltage output). During the measurement, the Ag/AgCl reference electrode was connected to the black cable of the source meter, and the PB/carbon sensing electrode together with the triboelectric electrode was connected to the red cable of the source meter. Mechanical stimuli were applied and measured using a lab-built setup based on a computer-controlled movable stage and a digital force gauge (M5, Mark-10).

Supporting Information

Supporting Information is available from the Wiley Online Library or from the author.

Acknowledgements

The authors acknowledge Seiya Ono for helpful discussions. This work was supported in part by the Bakar Fellows Program, the National Science Foundation under Grant No. 1610899, and FlexTech Alliance under Grant No. AFOSR 42299.

Conflict of Interest

The authors declare no conflict of interest.

Keywords

mechanoreceptors, potentiometric mode, self-adapting materials, single-mode output, triboelectric mode

Received: September 1, 2020

Revised: October 12, 2020

Published online:

- [1] A. Chortos, J. Liu, Z. Bao, *Nat. Mater.* **2016**, *15*, 937.
- [2] V. E. Abaira, D. D. Ginty, *Neuron* **2013**, *79*, 618.
- [3] R. S. Johansson, J. R. Flanagan, *Nat. Rev. Neurosci.* **2009**, *10*, 345.
- [4] M. L. Hammock, A. Chortos, B. C.-K. Tee, J. B.-H. Tok, Z. Bao, *Adv. Mater.* **2013**, *25*, 5997.
- [5] Y. Zang, F. Zhang, C. Di, D. Zhu, *Mater. Horiz.* **2015**, *2*, 140.
- [6] J. Li, R. Bao, J. Tao, Y. Peng, C. Pan, *J. Mater. Chem. C* **2018**, *6*, 11878.
- [7] J. Park, Y. Lee, M. Ha, S. Cho, H. Ko, *J. Mater. Chem. B* **2016**, *4*, 2999.
- [8] H. Chen, L. Miao, Z. Su, Y. Song, M. Han, X. Chen, X. Cheng, D. Chen, H. Zhang, *Nano Energy* **2017**, *40*, 65.
- [9] Q. Hua, J. Sun, H. Liu, R. O. Bao, R. Yu, J. Zhai, C. Pan, Z. L. Wang, *Nat. Commun.* **2018**, *9*, 244.
- [10] K.-Y. Chun, Y. J. Son, E.-S. Jeon, S. Lee, C.-S. Han, *Adv. Mater.* **2018**, *30*, 1706299.
- [11] C. M. Boutry, Y. Kaizawa, B. C. Schroeder, A. Chortos, A. Legrand, Z. Wang, J. Chang, P. Fox, Z. Bao, *Nat. Electron.* **2018**, *1*, 314.
- [12] J. Tolvanen, J. Hannu, H. Jantunen, *IEEE Sens. J.* **2017**, *17*, 4735.
- [13] J. Ge, L. Sun, F.-R. Zhang, Y. Zhang, L.-A. Shi, H.-Y. Zhao, H.-W. Zhu, H.-L. Jiang, S.-H. Yu, *Adv. Mater.* **2016**, *28*, 722.
- [14] D. J. Lipomi, M. Vosgueritchian, B. C. Tee, S. L. Hellstrom, J. A. Lee, C. H. Fox, Z. Bao, *Nat. Nanotechnol.* **2011**, *6*, 788.
- [15] J. Park, M. Kim, Y. Lee, H. S. Lee, H. Ko, *Sci. Adv.* **2015**, *1*, e1500661.
- [16] L. Lin, Y. Xie, S. Wang, W. Wu, S. Niu, X. Wen, Z. L. Wang, *ACS Nano* **2013**, *7*, 8266.
- [17] D.-I. Kim, T. Q. Trung, B.-U. Hwang, J.-S. Kim, S. Jeon, J. Bae, J.-J. Park, N.-E. Lee, *Sci. Rep.* **2015**, *5*, 12705.
- [18] M. Ha, S. Lim, J. Park, D.-S. Um, Y. Lee, H. Ko, *Adv. Funct. Mater.* **2015**, *25*, 2841.
- [19] X. Wu, M. Ahmed, Y. Khan, M. E. Payne, J. Zhu, C. Lu, J. W. Evans, A. C. Arias, *Sci. Adv.* **2020**, *6*, eaba1062.
- [20] Y. Yang, H. Zhang, Z.-H. Lin, Y. S. Zhou, Q. Jing, Y. Su, J. Yang, J. Chen, C. Hu, Z. L. Wang, *ACS Nano* **2013**, *7*, 9213.
- [21] S. W. Chen, X. Cao, N. Wang, L. Ma, H. R. Zhu, M. Willander, Y. Jie, Z. L. Wang, *Adv. Energy Mater.* **2017**, *7*, 1601255.
- [22] J.-G. Sun, T. N. Yang, I.-S. Kuo, J.-M. Wu, C.-Y. Wang, L.-J. Chen, *Nano Energy* **2017**, *32*, 180.
- [23] J. Chen, P. Ding, R. Pan, W. Xuan, D. Guo, Z. Ye, W. Yin, H. Jin, X. Wang, S. Dong, J. Luo, *Nano Energy* **2017**, *34*, 442.
- [24] Z. L. Wang, *ACS Nano* **2013**, *7*, 9533.
- [25] C. Zhang, W. Tang, C. Han, F. Fan, Z. L. Wang, *Adv. Mater.* **2014**, *26*, 3580.
- [26] M. Ha, S. Lim, S. Cho, Y. Lee, S. Na, C. Baig, H. Ko, *ACS Nano* **2018**, *12*, 3964.
- [27] Z. L. Wang, J. Chen, L. Lin, *Energy Environ. Sci.* **2015**, *8*, 2250.
- [28] Z. Lin, J. Chen, J. Yang, *J. Nanomater.* **2016**, *2016*, 5651613.
- [29] J. Zhu, Y. Zhu, X. Wang, *Adv. Mater. Interfaces* **2018**, *5*, 1700750.
- [30] N. Kaur, K. Pal, *Energy Technol.* **2018**, *6*, 958.
- [31] X. Zhang, Y. Zheng, D. Wang, F. Zhou, *Nano Energy* **2017**, *40*, 95.
- [32] D. Rus, M. T. Tolley, *Nature* **2015**, *521*, 467.
- [33] B. Shih, D. Shah, J. Li, T. G. Thuruthel, Y.-L. Park, F. Iida, Z. Bao, R. Kramer-Bottiglio, M. T. Tolley, *Sci. Rob.* **2020**, *5*, eaaz9239.
- [34] X. Wu, Y. Khan, J. Ting, J. Zhu, S. Ono, X. Zhang, S. Du, J. W. Evans, C. Lu, A. C. Arias, *Adv. Electron. Mater.* **2020**, *6*, 1901310.
- [35] F.-R. Fan, L. Lin, G. Zhu, W. Wu, R. Zhang, Z. L. Wang, *Nano Lett* **2012**, *12*, 3109.
- [36] L. Zhao, Q. Zheng, H. Ouyang, H. Li, L. Yan, B. Shi, Z. Li, *Nano Energy* **2016**, *28*, 172.